

Universiteit
Leiden
The Netherlands

Cancer chess: molecular insights into PARP inhibitor resistance

Barazas, M.

Citation
Barazas, M. (2021, December 14). *Cancer chess: molecular insights into PARP inhibitor resistance*. Retrieved from https://hdl.handle.net/1887/3247064

Version:	Publisher's Version
License:	Licence agreement concerning inclusion of doctoral thesis in the Institutional Repository of the University of Leiden
Downloaded from:	https://hdl.handle.net/1887/3247064

Note: To cite this publication please use the final published version (if applicable).

Abstract

Poly(ADP-ribose) polymerase inhibition (PARPi) is a promising new therapeutic approach for the treatment of cancers that show homologous recombination deficiency (HRD). Despite the success of PARPi in targeting HRD in tumors that lack the tumor suppressor function of BRCA1 or BRCA2, drug resistance poses a major obstacle. We developed three-dimensional cancer organoids derived from genetically engineered mouse models (GEMMs) for BRCA1- and BRCA2-deficient cancers. Unlike conventional cell lines or mammospheres, organoid cultures can be efficiently derived and rapidly expanded *in vitro*. Orthotopically transplanted organoids give rise to mammary tumors that recapitulate the epithelial morphology and preserve the drug response of the original tumor. Notably, GEMM-tumor-derived organoids can be easily genetically modified, making them a powerful tool for genetic studies of tumor biology and drug resistance.

Cancer Chess:

BRCA-Deficient Mouse Mammary

Molecular Insights

Tumor Organoids to Study

Into PARPi Resistance

Cancer Drug Resistance

Chapter 3

Adapted from:

Alexandra A Duarte, Ewa Gogola, Norman Sachs, ***Marco Barazas****, Stefano Annunziato, et al.*

Nature Methods. 15(2):134-140 (2018)

Introduction

We have previously demonstrated that mammary adenocarcinomas that arise in *K14cre;Brca1$^{F/F}$;p53$^{F/F}$* (KB1P), *K14cre;Brca1$^{F/F}$; p53$^{F/F}$;Mdr1a/b$^{-/-}$* (KB1PM) and *K14cre;Brca2$^{F/F}$; p53$^{F/F}$* (KB2P) mouse models of BRCA-associated hereditary breast cancer recapitulate key features of the human disease [1, 2], including morphology, expression of basal markers, genomic instability and hypersensitivity to DNA-targeting therapy [3]. These features are preserved following orthotopic transplantation of tumor fragments into syngeneic mice [4]. This transplantation model has proven to be useful for studying mechanisms of drug resistance, particularly to PARP inhibitors [5-10]. To perform detailed analyses of drug resistance mechanisms, we derived two-dimensional (2D) cell lines from KB1P(M) and KB2P mammary tumors [6, 11]. Although these cell lines are useful, they exhibit limitations such as phenotypic and genetic uniformity and divergence from the primary tumor during adaptation to *in vitro* growth.

Recently, *in vitro* culture methods have been developed for efficient derivation of three-dimensional (3D) organoids from normal and malignant tissue [12, 13]. Organoid cultures preserve important features of the original tumor, such as cellular heterogeneity and self-renewal capacity. We developed a panel of KB1P(M) and KB2P tumor-derived organoid lines that provide more physiological models in which to study drug resistance than 2D cultures. We used pairs of PARPi-sensitive and PARPi-resistant BRCA1- and BRCA2-deficient tumors to test whether organoid cultures can be used to predict the drug response of the original tumor both *in vitro* and after orthotopic transplantation into mice.

Results

Generation of mammary tumor organoids

We adapted a previously described culture system [12] to both fresh and cryopreserved mammary tumor tissues, yielding mammary tumor organoid cultures that could be rapidly expanded and cultured *in vitro* (Supplementary Fig. 1A). The success rate for establishing organoid lines was high for both KB1P(M) and KB2P donor tumors, whereas previous attempts to derive 2D cell lines or 3D mammospheres were much less efficient (Fig. 1A). Similar success rates were obtained for the *K14cre;p53$^{F/F}$* (KP) and *K14cre;p53$^{F/F}$;Mdr1a/b$^{-/-}$* (KPM) models, which were used as a BRCA-proficient control. Stable organoid lines could be obtained in 2–3 weeks, whereas 2D cell lines required 3–6 months to adapt to *in vitro* conditions. Moreover, KB1P(M)/KB2P organoid lines could be cultured under normal oxygen conditions, whereas BRCA1- and BRCA2-deficient cell lines require a 3% oxygen environment. The success rate of orthotopic transplantation of KB1P(M)/KB2P organoids was high: we observed tumor outgrowth for all of the organoid lines tested (nine KB1P(M) and ten KB2P organoid lines; data not shown).

To assess the potential of mammary carcinoma organoids to form tumors *in vivo*, we performed a limiting dilution experiment in which we injected 100–1,000,000 cells (as organoids) of the PARPi-naive KB1P4 organoid line (ORG-KB1P4N.1) in the mammary fat pad of wild-type mice. We observed consistent tumor development in animals transplanted with as few as 1,000 cells (Fig. 1A), demonstrating the high tumorigenic potential of these cells compared with conventional cell lines that require transplantation of 0.5–1 × 10^6 cells [6]. Tumor latency of transplanted organoids correlated with the number of cells transplanted, suggesting that organoids undergo polyclonal expansion *in vivo* (Supplementary Table 1). The tumorigenic potential of KB1P(M) and KB2P organoids did not result from *in vitro* transformation, as organoids isolated from healthy mammary tissue (Supplementary Fig. 1B) did not give rise to mammary tumors following transplantation (Supplementary Table 1), despite the fact that normal mammary organoids and tumor organoids showed similar proliferation rates *in vitro* (Supplementary Fig. 1C).

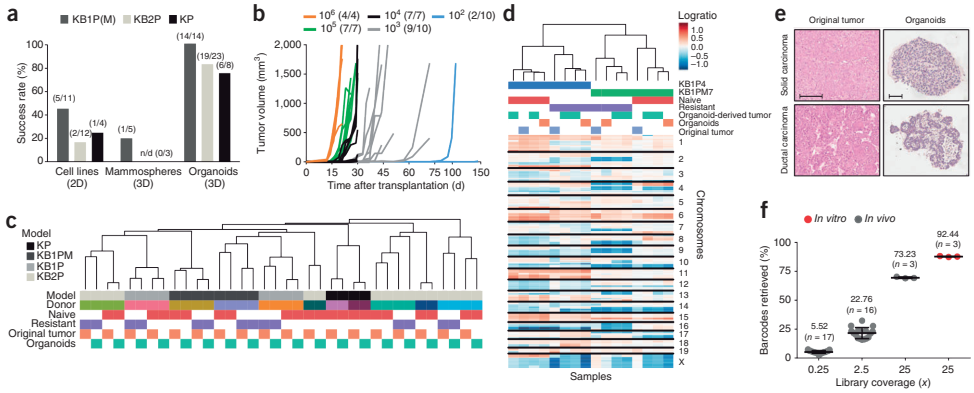


FIGURE 1 | Generation and characterization of mouse mammary tumor organoids. *(A)* Success rates for establishing 2D and 3D *in vitro* models from the indicated mammary tumors. Values in brackets indicate the number of donor tumors from which models were successfully derived versus the total number of donor tumors. n.d., no data. *(B)* Tumorigenic potential of organoids *in vivo*. Animals were transplanted with 10^2–10^6 organoid cells and tumor growth was monitored. Values in brackets indicate the number of tumors obtained versus the total number of mammary fat pads injected. *(C)* Unsupervised hierarchical clustering based on DNA copy number profiles of a panel of 18 organoid lines and their respective original GEMM tumors (correlation distance, average linkage). Tested models and individual donors are represented by different colors (Supplementary Fig. 3A). *(D)* Unsupervised hierarchical clustering based on DNA copy number profiles of a representative panel of four original KB1P(M) tumors, organoids and organoid-derived tumors (correlation distance, complete linkage). *(E)* Tumor-derived organoids preserve the morphology of the donor tumor. Scale bars represent 100 µm. *(F)* Quantification of barcodes retrieved from ORG-KB1PM7N.1 organoid cells transduced with a lentiviral library of 20,000 barcodes (*in vitro* sample) and tumors obtained following organoid transplantation (*in vivo* samples). The fraction of barcodes retrieved by genomic sequencing is represented as a function of the theoretical library coverage. The average library fraction retrieved is indicated. *in vitro*: *n* represents the number of replicates (samples); *in vivo*: *n* represents the number of tumors.

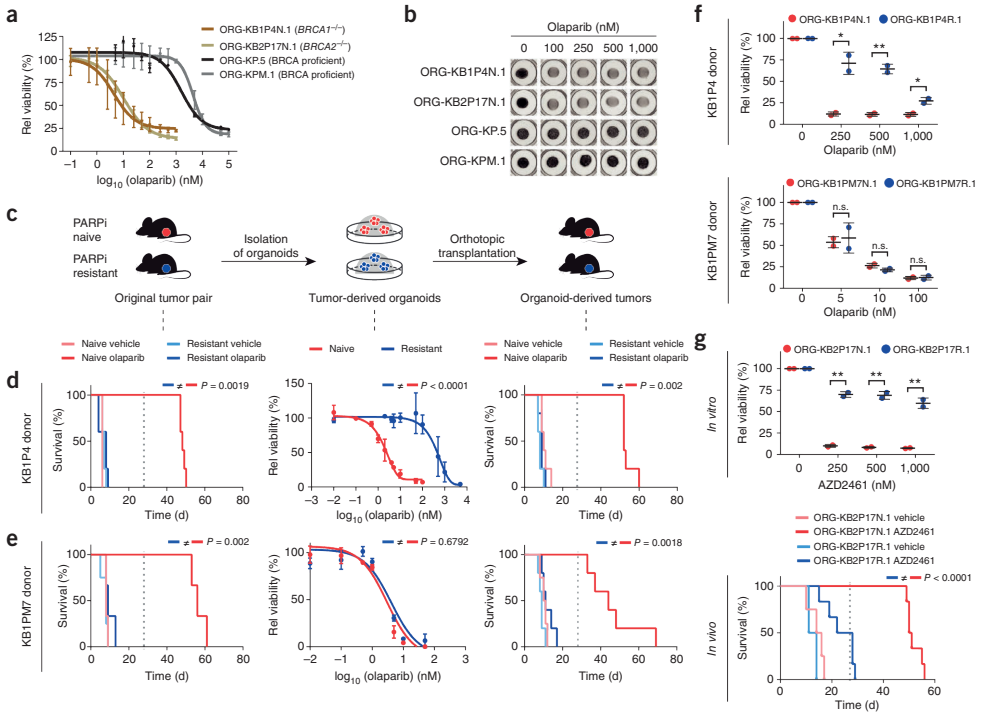


FIGURE 2 | Comparison of PARPi response of original GEMM tumors, tumor-derived organoids and organoid-derived tumors. *(A-B) In vitro* responses of BRCA-deficient and BRCA-proficient organoids to the PARP inhibitor olaparib. Quantification *A* and representative images of stained wells *B* are shown. Data represent two independent experiments. *(C)* General outline. *(D-E) In vivo* and *in vitro* PARPi response of models derived from KB1P4 *D* and KB1PM7 *E* donor tumors. Left, Kaplan–Meier curves showing the survival of mice bearing the original tumors treated with either vehicle or Olaparib for 28 consecutive days (KB1P4 donor: *n* = 2 for naive vehicle, *n* = 5 for other treatment groups; KB1PM7 donor: *n* = 4 for resistant vehicle, *n* = 3 for other treatment groups). End of treatment is indicated by a dotted grid line. *P* values were calculated by log-rank test (Mantel–Cox). Middle, *in vitro* olaparib response of ORG-KB1P4N.1/R.1 and ORG-KB1PM7N.1/R.1 organoids, as determined by a viability assay. Data are presented as mean ± s.d. for two independent replicates; value was calculated with extra sum-square F test. Right, Kaplan–Meier curves showing survival of mice transplanted with the same organoids (*n* = 5 per treatment group) (Supplementary Fig. 6). *(F) In vitro* PARPi toxicity in ORG-KB1P4N.1/R.1 (top) and ORG-KB1PM7N.1/R.1 (bottom) organoids as determined using a long-term clonogenic assay. Data are presented as the mean ± s.d. of two independent experiments. **P* < 0.01, ***P* < 0.001 (*t* test); n.s., not significant. *(G) In vitro* and *in vivo* responses of organoids derived from KB2P17 donor tumors to the PARPi AZD2461. Top, long-term clonogenic assay, data represented and analyzed as in *F*. Bottom, Kaplan–Meier survival curves, *P* value – log-rank Mantel–Cox test. Treatment of mice and survival analysis was carried out as described above (*n* = 4 for vehicle, *n* = 6 for AZD2461).

We next performed genetic and histological characterization of KB1P(M)/KB2P organoids and the corresponding tumor outgrowths to determine whether they retained the essential features of the parental GEMM tumors. As expected, deletions of *Brca1*, *Brca2*, *p53* and *Mdr1a* were conserved in both organoids and organoid-derived tumors, as confirmed by genotyping PCR (Supplementary Fig. 2). Given that BRCA-deficiency is strongly associated with high genomic instability [14], we generated DNA

copy number profiles for a panel of 18 organoid lines and their respective original tumors. Unsupervised hierarchical clustering revealed a high similarity between the patterns of genetic aberrations of organoids and their original donors (Fig. 1C and Supplementary Fig. 3A). As expected, BRCA-proficient KP tumors and organoid lines carried a substantially lower number of genetic aberrations than those lacking BRCA1 or BRCA2 function [15]. Moreover, the resemblance to the parental tumor was higher for organoids than for the 2D cell lines isolated from the same tumor (Supplementary Fig. 3B). We extended this analysis to organoid-derived tumors and observed that the genetic fingerprint of the organoids was maintained following transplantation (Fig. 1D). In addition, the epithelial phenotype that characterizes the KB1P(M) and KB2P tumor models was preserved following transplantation, as determined by morphology and immunohistochemistry (Fig. 1E and Supplementary Fig. 4).

To examine the cellular fitness of organoids *in vivo* and the clonal evolution of organoid-derived tumors, we barcoded individual cells in organoids by lentiviral transduction. Using transduction with a GFP-encoding lentivirus, we found that a multiplicity of infection (MOI, the number of viral particles per cell) of 1 resulted in about 30% of cells expressing GFP (Supplementary Fig. 5). This value increased to 68% when we applied an MOI of 5. We introduced a lentiviral library of 20,000 barcodes in the PARPi-naive KB1PM7 organoid line (ORG-KB1PM7N.1) at an MOI of 1. After puromycin selection, the barcoded organoids were transplanted into syngeneic wild-type mice at different cell numbers, corresponding to a theoretical library coverage of 0.25 to 25 (number of cells = theoretical coverage × library complexity). After outgrowth of the tumors, we purified and amplified the barcode-containing DNA. Using massive parallel sequencing, we quantified the barcodes to determine the fraction of the library present in the tumor cell population (Fig. 1F). After puromycin selection and before transplantation, an average of 92% of the barcodes could be retrieved from the organoid culture at a coverage of 25x. In the tumors that grew out, we still found 73% of the barcodes, indicating that a substantial fraction of the barcodes was preserved. At a coverage of 2.5x and 0.25x, this value decreased to approximately 23% and 6%, respectively. Taken together, these data suggest that GEMM-tumor-derived organoids exhibit high clonal heterogeneity *in vivo* and give rise to tumors that preserve the cellular complexity of the parental organoid population. We conclude that these models are suitable for studying the effects of intratumoral heterogeneity *in vivo* and are particularly compatible with *in vivo* screening approaches.

Analysis of PARPi response in vivo and in vitro

We determined the PARPi sensitivity of organoid cultures using a standard cytotoxicity assay. Consistent with the concept of synthetic lethal interaction between PARP1 inhibition and BRCA1 and BRCA2 deficiency [16], organoids derived from KB1P/KB2P tumors were more sensitive to treatment with the clinical PARP inhibitor olaparib

than homologous recombination (HR)-proficient KP(M) organoids (Fig. 2A-B). We next studied the *in vitro* and *in vivo* olaparib response of ORG-KB1P4N.1/R.1 and ORG-KB1PM7N.1/R.1 organoids, which were derived from two matched pairs of PARPi-naive and resistant tumors (Fig. 2C). For both KB1P4 and KB1PM7 donors, we found olaparib resistance to be stable following re-transplantation of the original tumor (Fig. 2D-E and Supplementary Fig. 6A-C). We examined the olaparib response in organoid lines *in vitro* and in parallel we transplanted the organoid lines orthotopically into wild-type animals and tested the olaparib response of the organoid-derived mammary tumors. Similar to the original KB1P4 olaparib-naive and olaparib-resistant tumors, ORG-KB1P4N.1 and its resistant derivative retained their differential sensitivities to PARPi treatment both *in vitro* and *in vivo* (Fig. 2D and Supplementary Fig. 6B). Tumors arising from ORG-KB1PM7N.1 and ORG-KB1PM7R.1 organoids also reproduced the respective olaparib-sensitive and olaparib-resistant phenotypes described for the donor tumors, demonstrating that organoid-derived tumors can recapitulate the PARPi response of the original tumors (Fig. 2E and Supplementary Fig. 6D). However, we did not observe a difference in olaparib sensitivity between ORG-KB1PM7N.1 and ORG-KB1PM7R.1 *in vitro* (Fig. 2E).

To investigate the long-term cytotoxic effects of PARPi treatment on organoid cultures, we performed an *in vitro* clonogenic assay. Although ORG-KB1P4N.1 and ORG-KB1P4R.1 exhibited significantly different olaparib responses, ORG-KB1PM7N.1 and ORG-KB1PM7R.1 failed to do so (Fig. 2F). In addition, we extended our analysis to ORG-KB2P17N.1/R.1 organoids derived from a matched pair of PARPi-naive and PARPi-resistant KB2P tumors that have been shown to preserve their drug response after re-transplantation [10]. Similar to KB1P4-derived organoids, following treatment with the PARPi AZD2461, ORG-KB2P17N.1/R.1 organoids recapitulated the PARPi-phenotype both *in vitro* and *in vivo* (Fig. 2G).

Given the low olaparib IC_{50} of the ORG-KB1PM7R.1 organoid line, the data suggest that these organoids are sensitized to PARPi *in vitro*. To exclude a potential effect of the WNT and EGFR pathways, which are activated by the organoid culture medium, we examined the drug response of ORG-KB1PM7N.1/R.1 and ORG-KB1P4N.1/R.1 organoids cultured in medium depleted of the critical growth factors R-spondin 1, Noggin and EGF. The PARPi-resistance phenotype of both organoid pairs was unaffected by the growth-factor-depleted medium (Supplementary Fig. 7A-B). These results were confirmed in two additional organoid pairs, ORG-KB1PM7N.2/R.2, which was independently isolated from the original KB1PM7N/R tumors (thereby excluding a possible clonal artifact), and ORG-KB1PM7N.3/R.3, which were both isolated from the vehicle-treated tumors that arose from transplantation of ORG-KB1PM7N.1/R.1 and which faithfully recapitulated the phenotype of the original donor tumors (Supplementary Fig. 7C). These findings demonstrate that some mechanisms of PARPi resistance in KB1P(M), and possibly KB2P, tumors are not effectively recapitulated by *in vitro* viability assays with tumor-derived organoids.

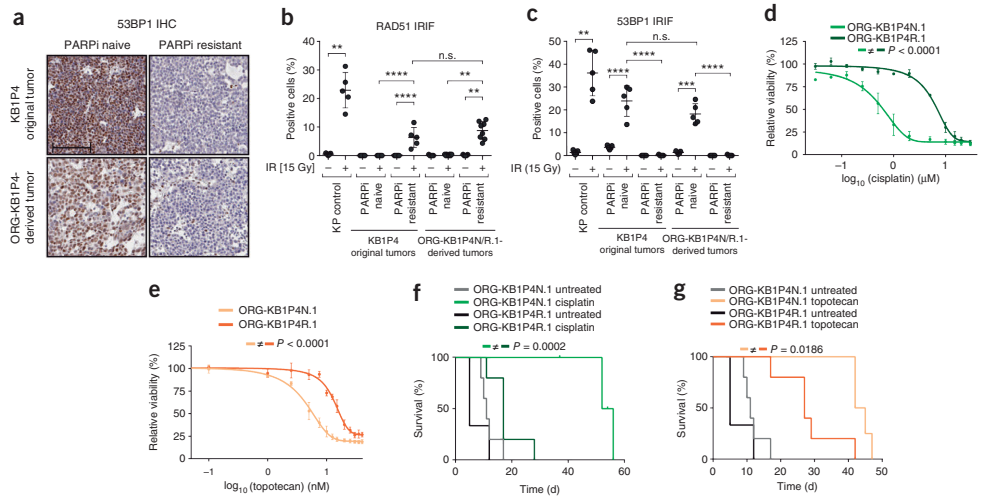


FIGURE 3 | PARPi-resistant GEMM-derived cancer organoids preserve functional properties of the original tumors. *(A)* Representative 53BP1 staining of the indicated tumors. Scale bar represents 100 μm. *(B) In situ* analysis of RAD51 IRIF formation in indicated tumors. KP tumor was used as a positive control. Cells with >5 nuclear foci were considered positive; each data point represents a single area of the tumor analyzed (>50 cells per area); ***P* < 0.001, ****P* < 0.0005, *****P* < 0.0001, *t* test. (**c**) 53BP1 IRIF formation assay, analyzed as described in *B*. *(D-E) In vitro* response of ORG-KB1P4N.1/R.1 organoids to cisplatin *D* and topotecan *E*. Data are presented as the mean ± s.d. of two independent repeats; *P* value, extra-sum square F test. *(F-G)* Overall survival (Kaplan–Meier curves) of mice transplanted with ORG-KB1P4N.1/R.1 organoids, untreated (ORG-KB1P4N.1/R.1, *n* = 5 and *n* = 3, respectively), or treated with cisplatin (ORG-KB1P4N.1/R.1, *n* = 5) *F* or topotecan (ORG-KB1P4N.1/R.1, *n* = 4 and *n* = 5, respectively) *G*. Cisplatin (6 mg/kg) was administered at days 0 and 14 and topotecan (4 mg/kg) was administered at days 0–4 and 14-18; *P* value, log-rank (Mantel–Cox) test.

Functional analysis of drug-resistance mechanisms

The tumors from which the PARPi-resistant organoid lines ORG-KB1P4R.1 and ORG-KB1PM7R.1 are derived differ in their mechanism of resistance. As we established by RAD51/53BP1 ionizing-radiation-induced foci (IRIF) formation assays and we confirmed by immunohistochemistry (Fig. 3A-C and Supplementary Fig. 8A), PARPi resistance in the KB1P4R tumor is likely caused by loss of 53BP1 protein expression, a well-defined mechanism of HR restoration [6, 17, 18]. In contrast, we did not detect HR restoration in the olaparib-resistant KB1PM7R tumor (data not shown). Tumors derived from transplantation of ORG-KB1P4R.1 organoids also lack 53BP1 expression and maintain the capacity to form RAD51 IRIF, indicating that organoid-derived tumors preserve the mechanism of PARPi resistance of the donor tumors (Fig. 3A-C and Supplementary Fig. 8A).

We and others have previously shown that 53BP1 loss and consequent restoration of HR activity reduces the hypersensitivity of BRCA1-deficient cells to other DNA-damaging agents, such as cisplatin and topotecan [6]. We therefore examined the response of ORG-KB1P4N.1/R.1 organoids to these anticancer drugs, both *in vitro* and

in vivo. As expected, 53BP1-deficient ORG-KB1P4R.1 organoids were less sensitive to both agents (Fig. 3D-G and Supplementary Fig. 8B-C). Together, these data indicate that GEMM-derived mammary tumor organoid models can be employed to study the response to multiple cytotoxic drugs and establish cross-resistance profiles.

Genome editing for in vivo analysis of drug response

Finally, we explored the utility of GEMM-derived mammary tumor organoids for rapid *in vivo* validation of candidate mediators of drug resistance. We employed the CRISPR/Cas9 system, which has already been successfully used for genetic manipulation of organoids derived from mouse intestine and kidney [19-22]. As a proof-of-concept demonstration, we inactivated *Trp53bp1* in PARPi-naive BRCA1-deficient mouse mammary tumor organoids (ORG-KB1PM7N.1) and examined the response to olaparib treatment *in vivo*. We targeted the murine *Trp53bp1* locus in ORG-KB1PM7N.1 organoids by simultaneous co-transduction with lentiviruses expressing Cas9 and a doxycycline-regulated single guide RNA (sgRNA) against *Trp53bp1*. The frequencies of insertions

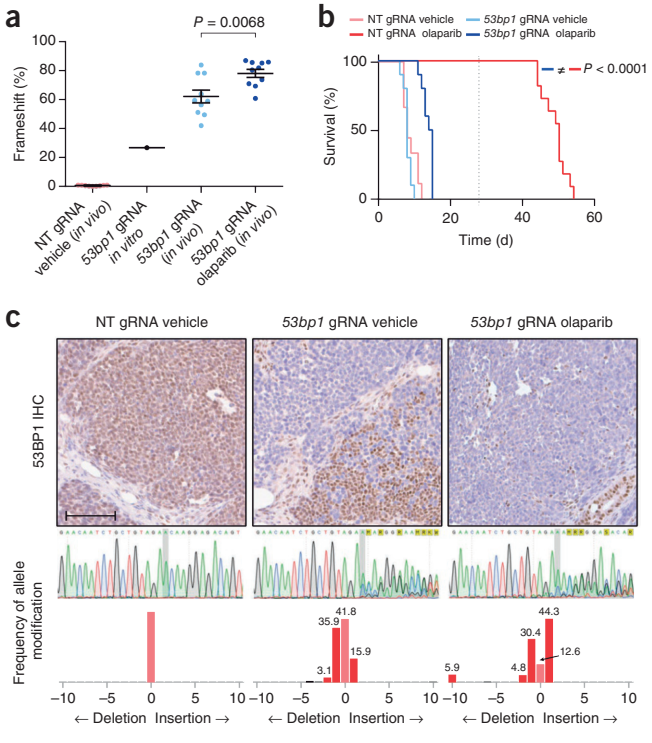


FIGURE 4 | Mouse mammary cancer organoids for *in vivo* validation of PARPi resistance factors. (*A*) Frequency of frameshift indels in *Trp53bp1* in manipulated organoids and organoid-derived tumors. *P* value was determined using the Student's *t* test. (*B*) Kaplan–Meier curves showing the survival of mice bearing tumors derived from ORG-KB1PM7N.1 organoids modified by CRISPR/Cas9 using a gRNA targeting *Trp53bp1* or a NT gRNA. Animals were treated with vehicle or olaparib for 28 consecutive days (n = 10 per treatment group). End of treatment is indicated by a dotted grid line (Supplementary Fig. 9). *P* value was calculated by log-rank test (Mantel–Cox). (*C*) Immunohistochemistry analysis of 53BP1 expression in tumors derived from the indicated organoids. Representative 53BP1 staining of tumors from each treatment group are shown with corresponding allele modification frequencies indicating the predicted indel size (bottom). Scale bar represents 100 µm.

and deletions (indels) were measured using the tracking of indels by decomposition (TIDE) method [23]. This analysis was performed after 7 days of doxycycline induction and revealed an indel frequency of 31% in *Trp53bp1*-targeted cells (data not shown), with a high proportion (27%) of *Trp53bp1* alleles carrying frameshift disruptions (Fig. 4A). As expected, tumors derived from transplantation of *Trp53bp1*-targeted ORG-KB1PM7N.1 organoids exhibited a limited response to olaparib compared with the control tumors (derived from ORG-KB1PM7N.1 organoids transduced with a non-targeting (NT) guide RNA (gRNA), which were highly sensitive (Fig. 4B and Supplementary Fig. 9). Frameshift mutations in the *Trp53bp1* locus were strongly enriched in vehicle-treated tumors (Fig. 4A), indicating that a loss of 53BP1 expression produces a substantial selective advantage in KB1PM tumor cells, even in the absence of PARPi treatment. We observed a further enrichment in *Trp53bp1* frameshift mutations following olaparib treatment, and immunohistochemical analysis confirmed the depletion of 53BP1-positive tumor cells (Fig. 4C). These data are consistent with the known role of 53BP1 loss in PARPi resistance. Notably, these results demonstrate that GEMM-derived mammary tumor organoids can be efficiently modified by the
CRISPR/Cas9 system to target a gene of interest. Moreover, *in vivo* characterization of targeted organoids can be readily performed as a result of the short latency period and efficient tumor outgrowth.

Discussion

We successfully combined our well-defined genetic mouse models of *BRCA1*- and *BRCA2*-mutated breast cancer with organoid culture technology. Preclinical models for BRCA1- and BRCA2-associated cancers have provided insight into mechanisms of drug resistance resulting from hypomorphic BRCA1 activity or genetic reversion of *BRCA1* and *BRCA2* genes (reviewed in [24]). Nevertheless, it is clear that restoration of BRCA1 and BRCA2 explains only some of the cases of therapy resistance in the clinic [25, 26]. The KB1P(M)/KB2P-derived mammary tumor organoids that we established here preserve the irreversible inactivation of BRCA1 and BRCA2 function. Thus, they are a powerful tool for studying and validating BRCA1- and BRCA2-independent mechanisms of anticancer drug resistance.

We previously generated unique and extensive panels of KB1P(M) and KB2P PARPi-resistant tumors with the potential to represent the tumor heterogeneity that is observed in human breast cancer [5, 6] (Gogola et al., unpublished data). Analyses of these tumor panels have elucidated previously unknown mechanisms of PARPi resistance, including increased ABCB1- and MDR1-mediated drug efflux and rewiring of the DNA repair machinery as a result of a loss of 53BP1 or REV7 and MAD2L2 [5-7]. Recent sequencing efforts of large panels of ovarian and breast cancers have shown that genetic alterations of ABCB1 and MDR1, 53BP1, and REV7 and MAD2L2 are indeed found in drug-resistant human tumors [26, 27]. In addition to their potential clinical

implications, studies using KB1P(M) and KB2P models also provide new insights into the basic mechanisms of DNA repair, as illustrated by a recent description of a previously unknown role for REV7 as a factor involved in NHEJ [8]. The study of organoids derived from these resistant tumors may be useful for identifying and targeting new vulnerabilities to overcome drug resistance.

As we demonstrated using CRISPR/Cas9-mediated inactivation of *Trp53bp1*, organoid lines derived from drug-naive tumors provide a rapid and straightforward model for testing candidate drug targets and therapy resistance genes. An increasing number of studies are employing high-throughput sequencing technologies to compile comprehensive descriptions of genetic aberrations in tumors. For example, whole-genome sequencing of 560 breast cancers identified a large number of somatic mutations in protein-coding cancer genes in tumors that show a mutational signature associated with BRCA1 or BRCA2 deficiency [15]. The effect of these somatic mutations on response to therapy could be systematically tested in our panel of KB1P(M) and KB2P tumor organoids.

As recently reviewed [28], 2D disease models have provided valuable knowledge on many cellular processes in cancer. However, clinical translation of drug candidates that show activity in 2D cancer cell lines has been poor, which is in part a result of the limitations of these *in vitro* models. GEMM-derived mammary tumor organoids retain critical characteristics of the original tumors and combine the ease of genetic manipulation with engraftment efficiency in syngeneic mice. These features render organoids especially suitable for genetic and pharmacologic screens *in vivo*.

Notably, in one case we found that organoids derived from a PARPi-resistant tumor displayed *in vitro* sensitivity to PARPi, whereas tumors derived from these organoids perfectly recapitulated the PARPi response observed in the original tumors *in vivo*. This finding points to the limitations of current 3D cancer organoids for studying drug resistance *in vitro* and highlights the need for additional studies to further improve 3D culture systems. The observed discrepancy between *in vitro* and *in vivo* responses to PARPi could be a result of a protective effect of the *in vivo* tumor microenvironment, which has been found to influence treatment response in breast cancer (reviewed in [29]). Thus, *in vivo* models remain important for studying therapy resistance. For this purpose, the generation of 3D cancer organoids and their genetic modification before orthotopic transplantation provides a unique tool for rapidly testing mechanisms of drug resistance *in vivo*.

Materials and Methods

A detailed step-by-step protocol, including the primary *in vitro* procedures with mouse mammary tumor organoids, is available through Protocol Exchange [30].

Establishment and maintenance of mammary tumor organoid lines

Fresh or cryopreserved mammary tumor pieces were minced and digested in Advanced DMEM/F12 medium (AdDMEM/F12, Gibco) supplemented with 5% FBS (vol/vol, Gibco), 2 mg/ml collagenase type IV (Gibco), 2 mg/ml trypsin (Difco), 5 µg/ml gentamicin (Invitrogen) and 5 µg/ml insulin (Sigma) for 30 min at 37 °C with gentle shaking. After centrifugation at 1,500 rpm for 10 min, the collagenase solution was discarded and the pellet was washed in AdDMEM/F12. The suspension was pelleted again, resuspended in 20 U/ml DNase (Roche) solution in AdDMEM/F12 and mixed by vortexing for 5 min. The DNase solution was discarded after centrifugation as before and the pellet was resuspended in AdDMEM/F12. The suspension was passed through a 70-µm cell strainer (Falcon), and washed once in AdDMEM/F12. Organoids were separated from single cells through multiple brief centrifugations at 1,500 rpm. Organoids were embedded in Cultrex Reduced Growth Factor Basement Membrane Extract Type 2 (BME, Trevigen), seeded on 24-well suspension plates (Greiner Bio-One) and cultured in complete mouse mammary gland organoid media (AdDMEM/F12 supplemented with 1 M HEPES (Sigma), GlutaMAX (Invitrogen), penicillin/streptomycin (Gibco), B27 (Gibco), 125 µM N-acetyl-l-cysteine (Sigma), 50 ng/ml murine epidermal growth factor (EGF, Invitrogen), 10% Rspo1-conditioned medium (vol/vol, kindly provided by C. Kuo, Stanford University) and 10% Noggin-conditioned medium[12] (vol/vol)). Organoids from healthy mammary tissue were isolated in a similar manner and cultured as described previously [31], with modifications. Healthy organoids were cultured in AdDMEM/F12 supplemented with 1 M HEPES, GlutaMAX, penicillin/streptomycin, 1% insulin-transferrin-selenium (vol/vol, Gibco) and 2.5 nM FGF2 (Sigma). Removal of FGF2 or incubation with tumor organoid media did not support growth of healthy organoids (data not shown).

Passaging of organoids was performed either via mechanical disruption using a fire-polished glass Pasteur pipet or by dissociation with TrypLE (Gibco). Passaging was performed weekly in a 1:2–1:6 ratio. For long-term storage, organoid cultures were dissociated and mixed with Recovery Cell Culture Freezing Medium (Gibco) and frozen following the standard procedures. When required, the organoids were thawed using standard thawing procedures, embedded in BME and cultured as described above.

Mice, generation of mammary tumors and orthotopic transplantations

All animal experiments were approved by the Animal Ethics Committee of The Netherlands Cancer Institute and performed in accordance with the Dutch Act on Animal Experimentation (November 2014). KP(M), KB1P(M) and KB2P mouse mammary tumors were generated as previously described [1, 5-7, 10]. Briefly, KP, KPM, KB1P, KB1PM and KB2P mammary tumors were generated in *K14cre;p53*$^{F/F}$, *K14cre;p53*$^{F/F}$*; Mdr1a/b*$^{-/-}$, *K14cre;Brca1*$^{F/F}$*;p53*$^{F/F}$, *K14cre;Brca1*$^{F/F}$*;p53*$^{F/F}$*; Mdr1a/b*$^{-/-}$ and *K14cre;Brca2*$^{F/F}$*;p53*$^{F/F}$ female mice, respectively. To generate PARPi-resistant tumors, KB1P(M) and KB2P tumors

were genotyped and orthotopically transplanted in wild-type FVB/N and FVB/Ola129 F1 mice, respectively. Mammary tumor size was determined by caliper measurements (length and width in millimeters), and tumor volume (in mm^3) was calculated by using the following formula: 0.5 × length × $width^2$. Upon KB1P tumor outgrowth to approximately 200 mm^3 (100%), mice were treated with vehicle, AZD2461 (100 mg/kg orally) or olaparib (50 mg/kg intraperitoneally) for 28 consecutive days. KB1PM tumor-bearing mice were similarly treated with olaparib and KB2P tumor-bearing mice were treated with AZD2461. Mice with a relapsing tumor received another treatment cycle when the tumor was 100% of the original size at treatment start. Animals were sacrificed with CO_2 when the tumor reached a volume of 1,500 mm^3.

For the transplantation of organoid lines, organoids were used at a size corresponding to an average of 150–200 cells per organoid. Organoid suspensions containing a total of 10^4 (KB1P(M)) or 5 × 10^4 (KB2P) cells were injected in the fourth right mammary fat pad of wild-type FVB/N (KB1P(M)) or NMRI nude (KB2P) mice. CRISPR/Cas9-manipulated organoids were transplanted in NMRI nude mice to prevent an immune response against Cas9 protein [32, 33]. Organoids were transplanted in complete mouse media/BME mixture (1:1).

Drugs and treatment of tumor-bearing mice

Treatment of mice transplanted with tumor pieces was initiated when tumors reached a size of approximately 200 mm^3. In animals transplanted with organoids, treatment was initiated when tumors reached a size of 75 mm^3 due to the accelerated growth of these tumors. Olaparib (100 mg/kg intraperitoneally) or AZD2461 (100 mg/kg orally) was administered for 28 consecutive days. To assess cross-resistance, mice were given a single treatment regimen of topotecan (4 mg/kg intraperitoneally, days 0–4 and 14–18) or cisplatin (6 mg/kg intravenously, days 0 and 14). Control mice were dosed with vehicle only. Mammary tumor size was determined as described above. Animals were sacrificed with CO_2 when the tumor volume reached 1,500 mm^3, unless otherwise stated. In addition to sterile collection of multiple tumor pieces for grafting experiments (as described above), tumor samples were frozen in dry ice and fixed in 4% formaldehyde solution in PBS (wt/vol).

Genotyping

Genomic DNA extraction from tumor and organoid samples was performed according to the standard phenol:chloroform extraction protocol. Genotyping of *Brca1*^{F}, *Brca1*, *Brca2*^{F}, *Brca2*, *p53* and *Mdr1a/b*$^{-/-}$ alleles was performed as previously described[1,2,6]. The *p53*^{F} allele was detected by PCR amplification with oligos Fwd-5'-GGGGAAGTTTCAAGCCTTCAT-3' and Rev-5'-TCTGAGAATCAGTTTATCCTCCCT-3', yielding products of 225 bp and 370 bp for the wild-type and *loxP*-flanked alleles, respectively.

The PCR reaction mix contained 100 ng of template DNA, 0.4 µM oligos and 5 µL MyTaq HS Red Mix (Bioline) in 10 µl total volume. Thermocycling conditions consisted of 30 s at 94 °C and 3 min at 60 °C.

Immunohistochemistry

Staining of E-cadherin, Vimentin, Keratin-14 and 53BP1 was performed on formalin-fixed paraffin-embedded (FFPE) tissue. Samples were boiled in Tris-EDTA pH 9.0 or citrate buffer pH 6.0 (53BP1) for antigen retrieval. Next, we used 3% H_2O_2 (vol/vol) in methanol to block endogenous peroxidase activity, and 10% milk (wt/vol, E-cadherin) or 4% BSA (wt/vol) plus 5% normal goat serum in PBS (vol/vol, Vimentin, 53BP1) as blocking buffer. Primary antibodies were diluted in 1.25% normal goat serum plus 1% BSA (wt/vol) in PBS. For detection and visualization, labeled polymer-HRP (horseradish peroxidase) anti-rabbit Envision (K4011, Dako), DAB (D5905, Sigma), H_2O_2 (A-31642, Sigma, 1:1,250) and hematoxylin counterstaining were applied. For staining, organoids were recovered from BME by washing with ice-cold PBS followed by centrifugation at 4 °C at 600 rpm for 5 min. After fixation in formalin, organoids were pelleted and embedded in 2% low-melting agarose (in PBS, Sigma). Staining was then performed as described above.

RAD51 and 53BP1 IRIF formation assay

For the analysis of RAD51 and 53BP1 IRIF, tumor pieces or organoids were transplanted into syngeneic mice. When tumors reached approximately 500 mm^3 in volume, the animals were either irradiated (15Gy) using a CT-guided high precision cone beam micro-irradiator (X-RAD 225Cx) or left untreated. 2 h after irradiation the tumors were taken out and fixed in 4% formalin. Immunofluorescent staining, foci visualization and analysis were carried out as described before [8]. A homologous recombination-proficient *K14cre;p53*$^{F/F}$ (KP) mammary tumor was used as positive control.

Antibodies

Primary antibodies: rabbit anti-E-cadherin (3195, Cell Signaling, 1:200); rabbit anti-Vimentin (5741, Cell Signaling, 1:200); rabbit anti-Keratin-14 (ab181595, Abcam, 1:6,000); rabbit anti-53BP1 (for immunohistochemistry, A300-272A, Bethyl Laboratories, 1:1,000; for immunofluorescence, ab21083, Abcam, 1:1,000); rabbit anti-RAD51 (kindly provided by R. Kanaar, Erasmus University Rotterdam).

Generation of DNA copy number profiles and data analysis

DNA copy number profiles were generated from whole exome sequencing (Fig. 1D and Supplementary Fig. 3B) or CNV-Seq data (Fig. 1C and Supplementary Fig. 3A). For

whole-exome sequencing, genomic DNA was sheared to approximately 300-bp fragments by sonication (Covaris S2), and 500–1,000 ng of sheared DNA was used as input for a six-cycle PCR to construct a fragmented library using the KAPA HTP Library Preparation Kit (Kapa). Exome enrichment was done using SureSelectXT2 Mouse All Exon kit (Agilent Technologies). The manufacturer's protocol (protocol G9630-90000) was followed except for the following steps: (1) the capture was diluted 1:1 and (2) six indexed samples were pooled before hybridization. Samples were sequenced on an Illumina HiSeq2500 (Illumina). DNA copy number profiles were generated from whole-exome sequencing data using CopyWriteR which uses off-target reads from the exome capture to estimate DNA copy number profiles [34]. DNA copy number profiles were generated using a bin size of 20,000 nucleotides. The $\log_2$-transformed read counts from CopyWriteR were used to cluster the samples using unsupervised hierarchical clustering (correlation distance, complete linkage). For visualization purposes, the heatmaps were drawn by down-sampling the original read counts to a bin size of 10,000,000 nucleotides; however, distances between samples were calculated using the original bin size of 20,000 nucleotides.

To perform CNV-Seq, the amount of double stranded DNA in the genomic DNA samples was quantified by using the Qubit dsDNA HS Assay Kit (Invitrogen, cat no Q32851). Up to 2,000 ng of double stranded genomic DNA were fragmented by Covaris shearing to obtain fragment sizes of 160–180 bp. Samples were purified using 1.8X Agencourt AMPure XP PCR Purification beads according to manufacturer's instructions (Beckman Coulter, cat no A63881). The sheared DNA samples were quantified and qualified on a BioAnalyzer system using the DNA7500 assay kit (Agilent Technologies cat no. 5067-1506). With a input of maximum 1 µg sheared DNA, library preparation for Illumina sequencing was performed using the KAPA HTP Library Preparation Kit (KAPA Biosystems, KK8234). During library enrichment 4–6 PCR cycles were used to obtain enough yield for sequencing. After library preparation, the libraries were cleaned up using 1× AMPure XP beads. All DNA libraries were analyzed on a BioAnalyzer system using the DNA7500 chips for determining the molarity. Up to 11 uniquely indexed samples were mixed together by equimolar pooling, in a final concentration of 10 nM, and subjected to sequencing on an Illlumina HiSeq2500 machine in one lane of a single-read 65-bp run, according to manufacturer's instructions. The resulting reads were aligned to the GRCm38 reference genome using BWA-MEM [35]. After the alignment, sample read counts were generated by counting aligned reads with a mapping quality ≥ 37 within 20-kb bins along the reference genome. These counts were then first corrected for GC bias using a nonlinear loess fit and second also corrected for mappability of the bins using a linear fit. Bins that overlapped regions blacklisted by Encode [36] or had a mappability below 0.2 were excluded from the final counts. Log ratios were determined by calculating the $\log_2$ ratio of each samples counts compared to a common reference count. This reference count was calculated using an in-silico simulated data set, in which simulated reads from the GRCm38 reference genome were

mapped and counted using the previously described approach and conditions. Finally, the samples were clustered by the $\log_2$ ratios using unsupervised hierarchical clustering (correlation distance, average linkage). For visualization purposes, the heatmaps were drawn by down-sampling the original read counts to a bin size of 10,000,000 nucleotides; however, distances between samples were calculated using the original bin size of 20,000 nucleotides.

Cell viability assay

For cell viability assays, organoids were dissociated into single cells as described above, and 50,000–100,000 cells were seeded per well in 40 µl complete mouse media/BME mixture on 24-well suspension plates and cultured for 7/14 (short/ long-term assay) days in the presence of a concentration range of olaparib, AZD2461, cisplatin or topotecan, as indicated. Cell viability was assessed by one of two methods: 1) using the resazurin-based Cell Titer Blue assay following manufacturer's protocol (Promega); or 2) via the ability of cellular oxidoreductase enzymes to reduce 3-(4,5-dimethylthiazol-2-yl)-2,5-diphenyltetrazolium bromide (MTT) to its insoluble, purple-colored formazan as previously described [37]. Briefly, MTT (Sigma) solution was added to the organoid culture to a final concentration of 500 mg/ml. After incubation for 2–3 h at 37 °C, the medium was discarded and 2% SDS (wt/vol, Biosolve) solution in PBS (Gibco) was added for 2 h to solubilize the BME matrix followed by addition of DMSO for 1 h to solubilize the reduced MTT. The OD was measured on a microplate absorbance reader (Tecan Infinite 200 PRO) at 562 nm. To assess cell proliferation, organoids were dissociated into single cells and seeded at 100,000 cells per well as described above; the Cell Titer Blue assay was performed at the indicated time points. All cell viability experiments were performed at least in duplicate and data were analyzed with GraphPad Prism statistical software using nonlinear regression and extra sum-of-squares F-test.

Organoid transduction

pLenti6-GFP (Invitrogen) was used as a transduction control. iKRUNC-Puro vector was created as described before [38], but instead of blasticidin resistance, a puro-mycin resistance ORF replaced the GFP ORF of FH1tUTG. The library of 20,000 barcodes was cloned into the iKRUNC-Puro vector (described elsewhere; Annunziato and Jonkers, unpublished data). The pGSC_Cas9_Neo vector was a kind gift from B. Evers (Netherlands Cancer Institute). For targeting of the murine *Tr53bp1* gene, the oligos Fwd-5'-CGAGGAACAATCTGCTGTAGAACA-3' and Rev-5'-AAACTGTTCTACAGCAGATTGTTC-3' were annealed and ligated to BfuAI-digested iKRUNC construct. The non-targeting gRNA was similarly cloned using the oligos Fwd-5'-CGAGTGATTGGGGGTCGTTCGCCA-3' and Rev-5'-AAACTGGCGAACGACCCCCAATCA-3'. All vectors were verified by Sanger sequencing and validated in KB1P tumor-derived cells (data not shown).

HEK293FT cells were used to generate cell-free viral supernatants. HEK293FT cells were cultured in IMDM (Sigma) supplemented with 10% FBS, 2 mM glutamine, and 50 U/ml penicillin/streptomycin. Lentiviral stocks, pseudotyped with the VSV-G envelope, were produced by transient co-transfection of four plasmids as previously described [39]. Viral titers were determined using qPCR Lentivirus Titration Kit (Applied Biological Materials).

For infection, organoids were incubated with TripLE at 37 °C for 10 min and then dissociated into single cells with a fire-polished glass pipette. Cells were pelleted at 1,200 rpm for 5 min, resuspended in virus suspension (in complete mouse media) and supplemented with 8 µg/ml Polybrene (Millipore). Viral transduction was performed by spinoculation as previously described [40]. For the barcode-labeled organoid experiment, the medium was refreshed twenty-four hours after infection and supplemented with 2 µg/ml puromycin (Gibco). For *Tr53bp1* knockout experiments, the medium was supplemented with 2 µg/ml puromycin and 500 µg/ml G418 (Gibco). Expression of sgRNAs was induced by treatment with 3 µg/ml doxycycline (Sigma) for 7 days.

Tr53bp1 sequence analysis

For validation of target modification, genomic DNA was isolated from tumor and organoid samples using Gentra Puregene (Qiagen) according to the manufacturer's recommendations. Following PCR amplification of *Tr53bp1* (Fwd-5'-TGAGAAATGGAGGCAACACCA-3' and Rev-5'-TGCAAATGTGGGCTACTGGG-3'), PCR products were sequenced (5'-CTCGATCTCACACTTCCGCC-3'). Allele modification frequencies were determined with the online Tracking of Indels by Decomposition (TIDE) software available at http://tide.nki.nl [23] using untransduced organoids as a reference sequence. The indel size ranges were set to 15 nucleotides upstream and downstream of the *Tr53bp1* target sequence.

Library representation analysis

To ensure single integration events following lentiviral transduction, the lentiviral titer was adjusted to yield 25% transduced cells (as determined by flow cytometry analysis following transduction with Lenti-GFP). Puromycin-resistant organoids were transplanted at different cell numbers per flank to achieve library coverage of 0.25*x*, 2.5*x* or 25*x* (cell number = library coverage × complexity). When tumors reached 1,000 mm^3 in volume, animals were sacrificed and whole tumors were snap frozen (dry ice). Following genomic DNA extraction (phenol:chloroform method), barcodes were retrieved by two rounds of PCR amplification using the following conditions: (1) 98 °C, 30 s, (2) 16 cycles of 98 °C for 10 s, 60 °C for 20 s and 72 °C for 1 min, (3) 72 °C, 5 min. Reaction mix consisted of 1.5 µl DMSO, 10 µl GC Phusion Buffer 5×, 1 µl 2 mM dNTPs,

0.25 µl 100 µM Fwd oligo, 0.25 µl 100 µM Rev oligo, 0.5µl Phusion polymerase in 50 µl total volume. As a template for PCR1, 12 µg of genomic DNA was used per sample (1 µg per reaction, 12 replicates per sample). Following PCR1 all replicates were pooled and 2.5µl was used as input for PCR2. Oligos used for PCR1: Fwd-5'-ACACTCTTTCCCTACACGACGCTCTTCCGATCTNNNNNNGGCTTTATATATCTTGTGGAAAGGACG-3', Rev-5'-GTGACTGGAGTTCAGACGTGTGCTCTTCCGATCTACTGACGGGCACCGGAGCCAATTCC-3' and PCR2: Fwd-5'-AATGATACGGCGACCACCGAGATCTACACTCTTTCCCTACACGACGCTCTTCCGATCT-3', Rev-5'-CAAGCAGAAGACGGCATACGAGATNNNNNNGTGACTGGAGTTCAGACGTGTGCTCTTCCGATCT-3'. NNNNNN represents one of the following six-nucleotide barcodes: CGTGAT, ACATCG, GCCTAA, TGGTCA, CACTGT, ATTGGC, GATCTG, TCAAGT, CTGATC, AAGCTA, GTAGCC, TACAAG, TTGACT, GGAACT, TGACAT, GGACGG, CTCTAC, GCGGAC, TTTCAC. Next, PCR2 products were purified using MinElute PCR Purification Kit (Qiagen) and sequenced (Illumina Sequencing 2500). Sequencing reads were aligned to the reference sequences using edgeR software (Bioconductor) [41].

Statistics

The following statistics were used for the indicated figures: Figures 2D,E,G (Kaplan-Meier curves), 3F,G and 4B, a log-rank Mantel-Cox test; Figures 2D,E and 3D,E and Supplementary Figure 7 (*in vitro* cytotoxic assays), nonlinear regression model was applied and *P* values were determined with extra sum-square F test; Figures 2F,G, 3B,C and 4A, a paired two-tailed *t*-test was used. All statistical analyses were performed with GraphPad Prism 6 software.

Statistics were calculated based on the following sample size: Figure 2D,E (left panel), KB1P4 donor: $n = 2$ for naive vehicle, $n = 5$ for other treatment groups, KB1PM7 donor: $n = 4$ for resistant vehicle, $n = 3$ for other treatment groups; Fig. 2D,E (right panel), ORG-KB1P4 and ORG-KB1PM7 donors: $n = 5$ per treatment group; Figure 2G (lower panel), ORG-KB2P17 donor: $n = 4$ for vehicle, $n = 6$ for AZD2461); Figure 3F,G, ORG-KB1P4 naive, $n = 5$ for vehicle, $n = 5$ for cisplatin and $n = 4$ for topotecan, ORG- KB1P4 resistant, $n = 3$ for vehicle, $n = 5$ for cisplatin and $n = 5$ for topotecan; Figure 4B, $n = 10$ per treatment group; Figures 2D,E (middle panel), 2F,G (upper panel), and 3D,E and Supplementary Figure 7, data are presented for two independent experiments (performed in duplicate).

Life Sciences Reporting Summary

Further information on experimental design is available in the Life Sciences Reporting Summary.

Data availability

The data that support the findings of this study not included as source data in this publication are available from the corresponding authors upon request. The deep sequencing data generated in this study are available in the European Nucleotide Archive (ENA) under accession number PRJEB22990 Source data for Figures 1–4 and Supplementary 1 and 7 are available online.

Acknowledgements

We wish to thank the members of the Preclinical Intervention Unit of the Mouse Clinic for Cancer and Ageing (MCCA) at the Netherlands Cancer Institute (NKI), N. Domanitskaia, N. Gerhards, G. Lakner, O. Levionnois, N. Regenscheit and M. Siffert (Vetsuisse Bern) for their technical support with the animal experiments. We are grateful to B. Evers (NKI) for providing the iKRUNC-Puro vector, H. van der Gulden (NKI) for her assistance with the genotyping procedure, and the NKI animal facility, animal pathology facility, flow cytometry facility and genomics core facility for their excellent service. Financial support came from the Dutch Cancer Society (KWF 2011-5220 and 2014-6532 to S.R. and J.J.), the Netherlands Organization for Scientific Research (VICI 91814643, Cancer Genomics Netherlands and a National Roadmap grant for Large-Scale Research Facilities to J.J., VENI 916.15.182 to N.S.), the Netherlands Genomics Initiative Zenith (93512009 to J.J.), the Swiss National Science Foundation (310030_156869 to S.R.), the Swiss Cancer Research Foundation (MD-PhD-3446-01-2014 to S.B.) and the European Union (ERC CoG-681572 to S.R. and ERC synergy grant 319661 COMBATCANCER to J.J.).

Author contributions

S.R., A.A.D. and E.G. conceived and designed the study. A.A.D., E.G. and N.S. developed and validated the mammary tumor organoid model with input from H.C. and help from J.M.H. For this purpose, they designed and conducted the experiments, and interpreted the results together with P.B., J.J. and S.R. M.B. and S.A. designed and performed the *in vivo* validation experiment using CRISPR/ Cas9-mediated targeting of 53BP1, analyzed the data and contributed to the figures. J.R.d.R. and A.V. carried out the bioinformatical analyses and provided the corresponding figures. S.B. and M.v.d.V. helped with animal studies. P.B., J.J. and S.R. supervised the project. A.A.D. and E.G. prepared the manuscript with input from all of the authors.

Disclosure of Potential Conflicts of Interest

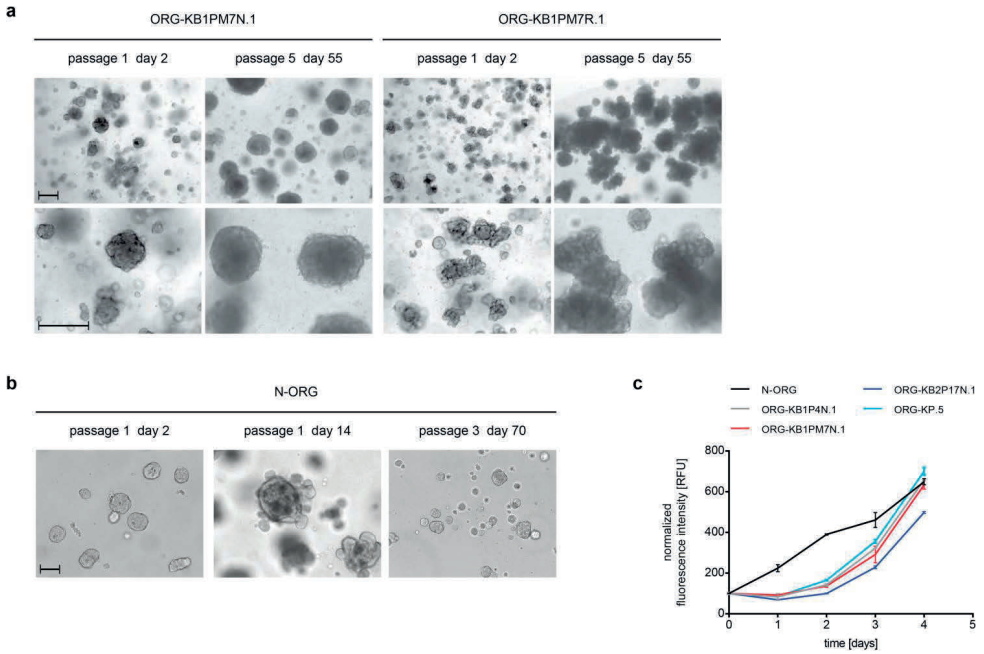
The authors declare that they have no competing financial interests.

References

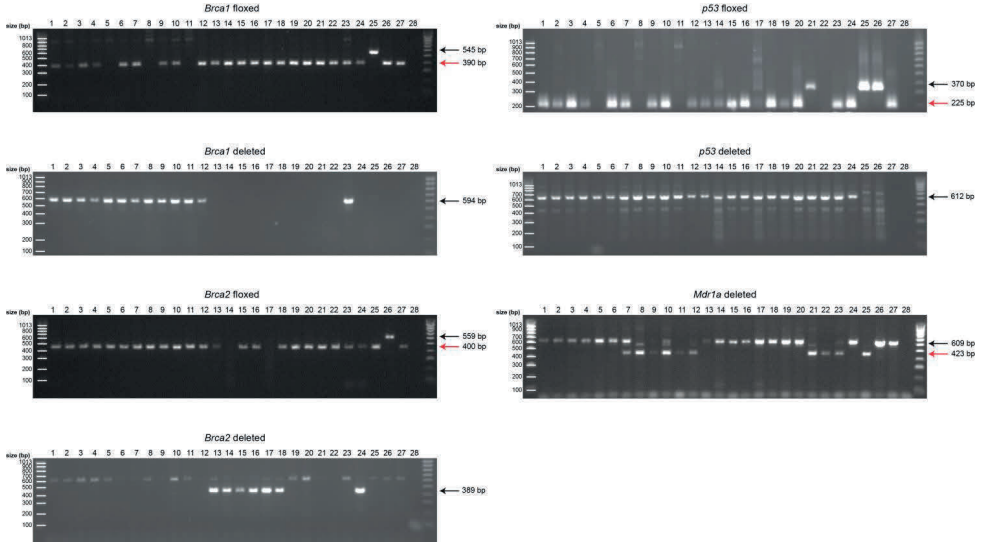
1. Jonkers J, Meuwissen R, van der Gulden H, Peterse H, van der Valk M, Berns A. Synergistic tumor suppressor activity of BRCA2 and p53 in a conditional mouse model for breast cancer. Nat Genet. 2001; 29: 418-25.
2. Liu X, Holstege H, van der Gulden H, Treur-Mulder M, Zevenhoven J, Velds A, et al. Somatic loss of BRCA1 and p53 in mice induces mammary tumors with features of human BRCA1-mutated basal-like breast cancer. Proc Natl Acad Sci U S A. 2007; 104: 12111-6.
3. Rottenberg S, Borst P. Drug resistance in the mouse cancer clinic. Drug Resist Updat. 2012; 15: 81-9.
4. Rottenberg S, Nygren AO, Pajic M, van Leeuwen FW, van der Heijden I, van de Wetering K, et al. Selective induction of chemotherapy resistance of mammary tumors in a conditional mouse model for hereditary breast cancer. Proc Natl Acad Sci U S A. 2007; 104: 12117-22.
5. Rottenberg S, Jaspers JE, Kersbergen A, van der Burg E, Nygren AO, Zander SA, et al. High sensitivity of BRCA1-deficient mammary tumors to the PARP inhibitor AZD2281 alone and in combination with platinum drugs. Proc Natl Acad Sci U S A. 2008; 105: 17079-84.
6. Jaspers JE, Kersbergen A, Boon U, Sol W, van Deemter L, Zander SA, et al. Loss of 53BP1 causes PARP inhibitor resistance in Brca1-mutated mouse mammary tumors. Cancer Discov. 2013; 3: 68-81.
7. Jaspers JE, Sol W, Kersbergen A, Schlicker A, Guyader C, Xu G, et al. BRCA2-deficient sarcomatoid mammary tumors exhibit multidrug resistance. Cancer research. 2015; 75: 732-41.
8. Xu G, Chapman JR, Brandsma I, Yuan J, Mistrik M, Bouwman P, et al. REV7 counteracts DNA double-strand break resection and affects PARP inhibition. Nature. 2015; 521: 541-4.
9. Tkáč J, Xu G, Adhikary H, Young JTF, Gallo D, Escribano-Díaz C, et al. HELB Is a Feedback Inhibitor of DNA End Resection. Mol Cell. 2016; 61: 405-18.
10. Ray Chaudhuri A, Callen E, Ding X, Gogola E, Duarte AA, Lee JE, et al. Replication fork stability confers chemoresistance in BRCA-deficient cells. Nature. 2016; 535: 382-7.
11. Evers B, Drost R, Schut E, de Bruin M, van der Burg E, Derksen PW, et al. Selective inhibition of BRCA2-deficient mammary tumor cell growth by AZD2281 and cisplatin. Clinical cancer research : an official journal of the American Association for Cancer Research. 2008; 14: 3916-25.
12. Sato T, Stange DE, Ferrante M, Vries RG, Van Es JH, Van den Brink S, et al. Long-term expansion of epithelial organoids from human colon, adenoma, adenocarcinoma, and Barrett's epithelium. Gastroenterology. 2011; 141: 1762-72.
13. Sato T, Vries RG, Snippert HJ, van de Wetering M, Barker N, Stange DE, et al. Single Lgr5 stem cells build crypt-villus structures in vitro without a mesenchymal niche. Nature. 2009; 459: 262-5.
14. Turner N, Tutt A, Ashworth A. Hallmarks of 'BRCAness' in sporadic cancers. Nat Rev Cancer. 2004; 4: 814-9.
15. Nik-Zainal S, Davies H, Staaf J, Ramakrishna M, Glodzik D, Zou X, et al. Landscape of somatic mutations in 560 breast cancer whole-genome sequences. Nature. 2016; 534: 47-54.
16. Ashworth A. A synthetic lethal therapeutic approach: poly(ADP) ribose polymerase inhibitors for the treatment of cancers deficient in DNA double-strand break repair. J Clin Oncol. 2008; 26: 3785-90.
17. Bouwman P, Aly A, Escandell JM, Pieterse M, Bartkova J, van der Gulden H, et al. 53BP1 loss rescues BRCA1 deficiency and is associated with triple-negative and BRCA-mutated breast cancers. Nat Struct Mol Biol. 2010; 17: 688-95.
18. Bunting SF, Callén E, Wong N, Chen HT, Polato F, Gunn A, et al. 53BP1 inhibits homologous recombination in Brca1-deficient cells by blocking resection of DNA breaks. Cell. 2010; 141: 243-54.
19. Schwank G, Koo BK, Sasselli V, Dekkers JF, Heo I, Demircan T, et al. Functional repair of CFTR by CRISPR/Cas9 in intestinal stem cell organoids of cystic fibrosis patients. Cell Stem Cell. 2013; 13: 653-8.
20. Matano M, Date S, Shimokawa M, Takano A, Fujii M, Ohta Y, et al. Modeling colorectal cancer using CRISPR-Cas9-mediated engineering of human intestinal organoids. Nat Med. 2015; 21: 256-62.
21. Drost J, van Jaarsveld RH, Ponsioen B, Zimberlin C, van Boxtel R, Buijs A, et al. Sequential cancer mutations in cultured human intestinal stem cells. Nature. 2015; 521: 43-7.
22. Freedman BS, Brooks CR, Lam AQ, Fu H, Morizane R, Agrawal V, et al. Modelling kidney disease with CRISPR-mutant kidney organoids derived from human pluripotent epiblast spheroids. Nat Commun. 2015; 6: 8715.

23. Brinkman EK, Chen T, Amendola M, van Steensel B. Easy quantitative assessment of genome editing by sequence trace decomposition. Nucleic Acids Res. 2014; 42: e168.
24. Annunziato S, Barazas M, Rottenberg S, Jonkers J. Genetic Dissection of Cancer Development, Therapy Response, and Resistance in Mouse Models of Breast Cancer. Cold Spring Harb Symp Quant Biol. 2016; 81: 141-50.
25. Ang JE, Gourley C, Powell CB, High H, Shapira-Frommer R, Castonguay V, et al. Efficacy of chemotherapy in BRCA1/2 mutation carrier ovarian cancer in the setting of PARP inhibitor resistance: a multi-institutional study. Clinical cancer research : an official journal of the American Association for Cancer Research. 2013; 19: 5485-93.
26. Patch AM, Christie EL, Etemadmoghadam D, Garsed DW, George J, Fereday S, et al. Whole-genome characterization of chemoresistant ovarian cancer. Nature. 2015; 521: 489-94.
27. Bruna A, Rueda OM, Greenwood W, Batra AS, Callari M, Batra RN, et al. A Biobank of Breast Cancer Explants with Preserved Intra-tumor Heterogeneity to Screen Anticancer Compounds. Cell. 2016; 167: 260-74.e22.
28. Horvath P, Aulner N, Bickle M, Davies AM, Nery ED, Ebner D, et al. Screening out irrelevant cell-based models of disease. Nat Rev Drug Discov. 2016; 15: 751-69.
29. McMillin DW, Negri JM, Mitsiades CS. The role of tumour-stromal interactions in modifying drug response: challenges and opportunities. Nat Rev Drug Discov. 2013; 12: 217-28.
30. Duarte AA, Gogola E, Sachs N, Barazas M, Annunziato S, J RdR, et al. BRCA-deficient mouse mammary tumor organoids to study cancer-drug resistance. Nat Methods. 2018; 15: 134-40.
31. Ewald AJ, Brenot A, Duong M, Chan BS, Werb Z. Collective epithelial migration and cell rearrangements drive mammary branching morphogenesis. Dev Cell. 2008; 14: 570-81.
32. Annunziato S, Kas SM, Nethe M, Yücel H, Del Bravo J, Pritchard C, et al. Modeling invasive lobular breast carcinoma by CRISPR/Cas9-mediated somatic genome editing of the mammary gland. Genes Dev. 2016; 30: 1470-80.
33. Wang D, Mou H, Li S, Li Y, Hough S, Tran K, et al. Adenovirus-Mediated Somatic Genome Editing of Pten by CRISPR/Cas9 in Mouse Liver in Spite of Cas9-Specific Immune Responses. Hum Gene Ther. 2015; 26: 432-42.
34. Kuilman T, Velds A, Kemper K, Ranzani M, Bombardelli L, Hoogstraat M, et al. CopywriteR: DNA copy number detection from off-target sequence data. Genome Biology. 2015; 16: 49.
35. Li HW. Aligning sequence reads, clone sequences and assembly contigs with BWA-MEM. arXiv: Genomics. 2013.
36. An integrated encyclopedia of DNA elements in the human genome. Nature. 2012; 489: 57-74.
37. Grabinger T, Luks L, Kostadinova F, Zimberlin C, Medema JP, Leist M, et al. Ex vivo culture of intestinal crypt organoids as a model system for assessing cell death induction in intestinal epithelial cells and enteropathy. Cell Death & Disease. 2014; 5: e1228-e.
38. Prahallad A, Heynen GJ, Germano G, Willems SM, Evers B, Vecchione L, et al. PTPN11 Is a Central Node in Intrinsic and Acquired Resistance to Targeted Cancer Drugs. Cell Rep. 2015; 12: 1978-85.
39. Follenzi A, Ailles LE, Bakovic S, Geuna M, Naldini L. Gene transfer by lentiviral vectors is limited by nuclear translocation and rescued by HIV-1 pol sequences. Nat Genet. 2000; 25: 217-22.
40. Koo BK, Stange DE, Sato T, Karthaus W, Farin HF, Huch M, et al. Controlled gene expression in primary Lgr5 organoid cultures. Nat Methods. 2011; 9: 81-3.
41. Robinson MD, McCarthy DJ, Smyth GK. edgeR: a Bioconductor package for differential expression analysis of digital gene expression data. Bioinformatics. 2010; 26: 139-40.

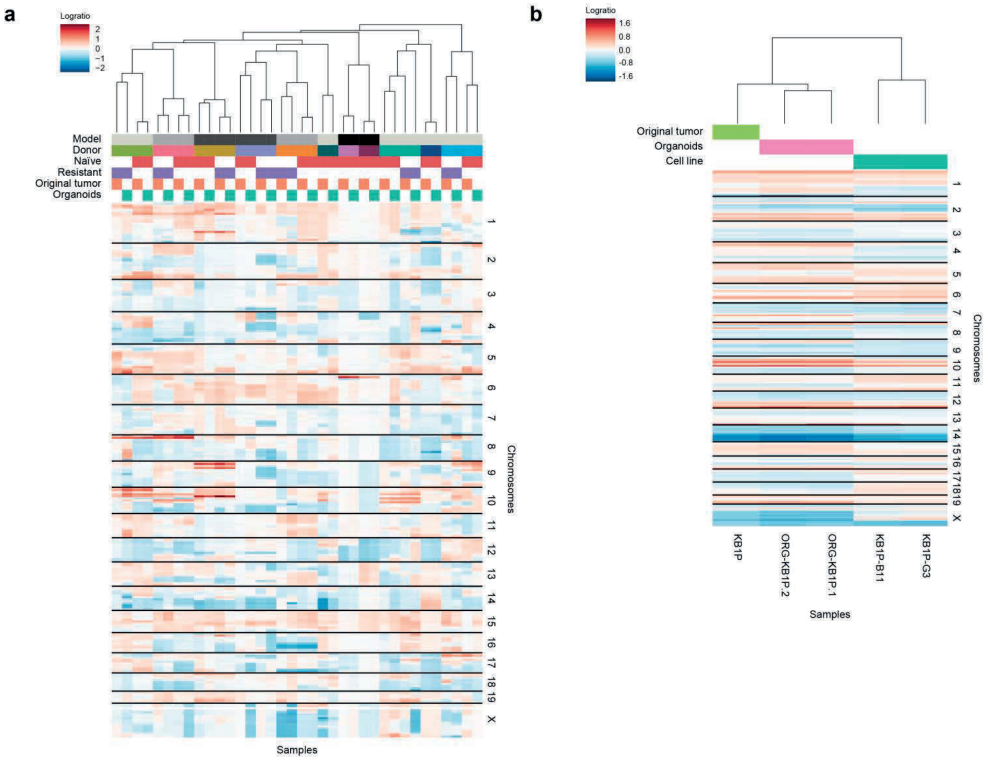
Supplementary Figures and Table



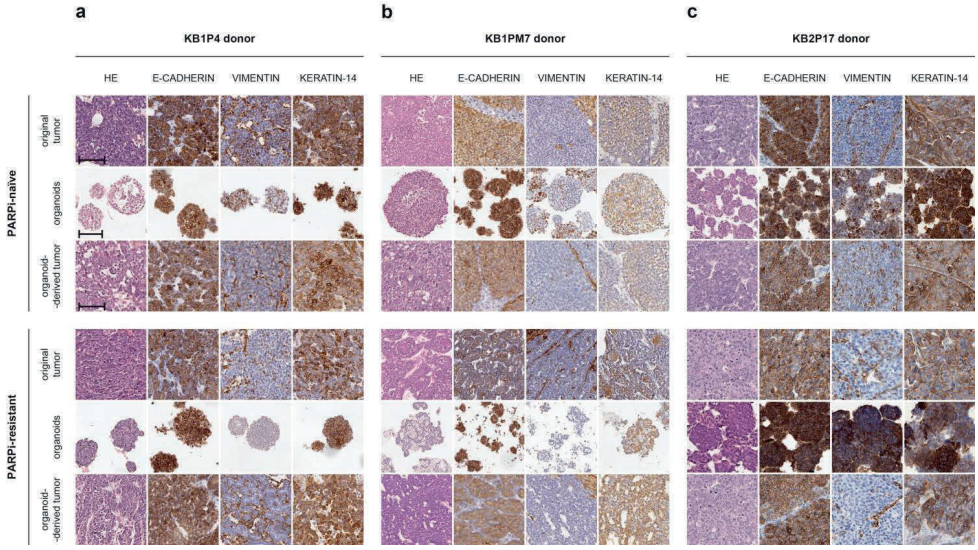
SUPPLEMENTARY FIGURE 1 | Comparison of mouse mammary organoids derived from malignant and healthy tissues. *(A)* Brightfield images of ORG-KB1PM7N.1/R.1 organoid cultures embedded in Basement Membrane Extract 2 days (passage 1) and 55 days (passage 5) following isolation. Scale bar, 100 µm. *(B)* Brightfield images of *in vitro* cultures of organoids derived from healthy mammary tissue (N-ORG) at the indicated time points. Scale bar, 100 µm. *(C) In vitro* proliferation of tumor (ORG-KP.5, ORG- KB1P4N.1, ORG-KB1PM7N.1 and KB2P17N.1) and healthy (N-ORG) mammary organoids, as determined by a cell viability assay.



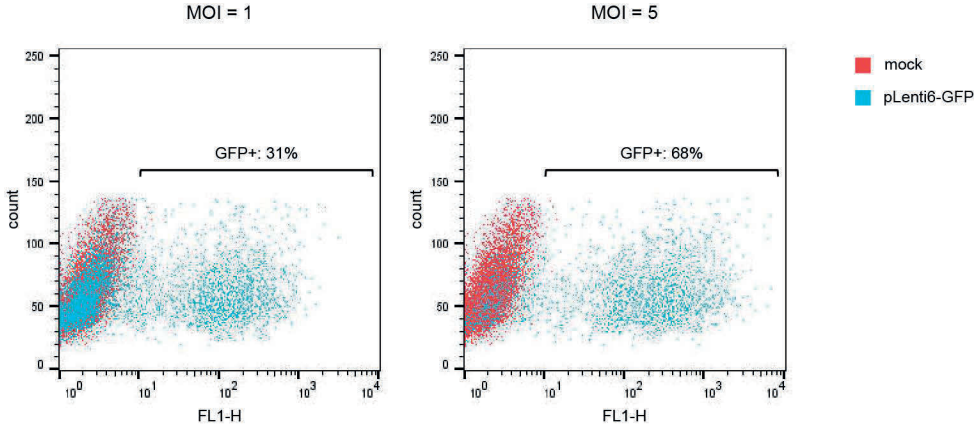
SUPPLEMENTARY FIGURE 2 | Genetic characterization of mouse mammary tumor organoids. Genotyping PCR of genomic DNA from KB1PM7, KB1P4, KB2P17, KP.5 and KPM.1 GEMM tumors, tumor-derived organoids and organoid-derived tumors. Wild-type bands are indicated by red arrows and floxed or deletion bands are indicated by black arrows. Wild- type bands indicate the presence of stromal cells from the syngeneic wild-type mice in which tumors were transplanted. Spleen DNA from KB1PM or KB2P mice was used as a positive control for the floxed PCR products and liver DNA from a wildtype animal was used as a positive control for the wild-type PCR products. Sample annotations: (1) KB1P4 naïve original tumor, (2) ORG-KB1P4N.1, (3) ORG-KB1P4N.1-derived tumor, (4) KB1P4 PARPi-resistant original tumor, (5) ORG-KB1P4R.1, (6) ORG-KB1P4R.1-derived tumor, (7) KB1PM7 PARPi-naïve original tumor, (8) ORG-KB1PM7N.1, (9) ORG-KB1PM7N.1-derived tumor, (10) KB1PM7 PARPi-resistant original tumor, (11) ORG-KB1PM7R.1, (12) ORG-KB1PM7R.1-derived tumor, (13) KB2P17 PARPi-naïve original tumor, (14) ORG-KB2P17N.1, (15) ORG-KB2P17N.1-derived tumor, (16) KB2P17 PARPi-resistant original tumor, (17) ORG-KB2P17R.1, (18) ORG-KB2P17R.1-derived tumor, (19) KP.5 original tumor, (20) ORG-KP.5, (21) KPM.1 original spontaneous tumor, (22) ORG-KPM.1, (23) KB1PM tumor (positive control), (24) KB2P tumor (positive control), (25) KB1PM spleen (floxed control), (26) KB2P spleen (floxed control), (27) wild-type liver (wild-type control), (28) negative control (no DNA input).



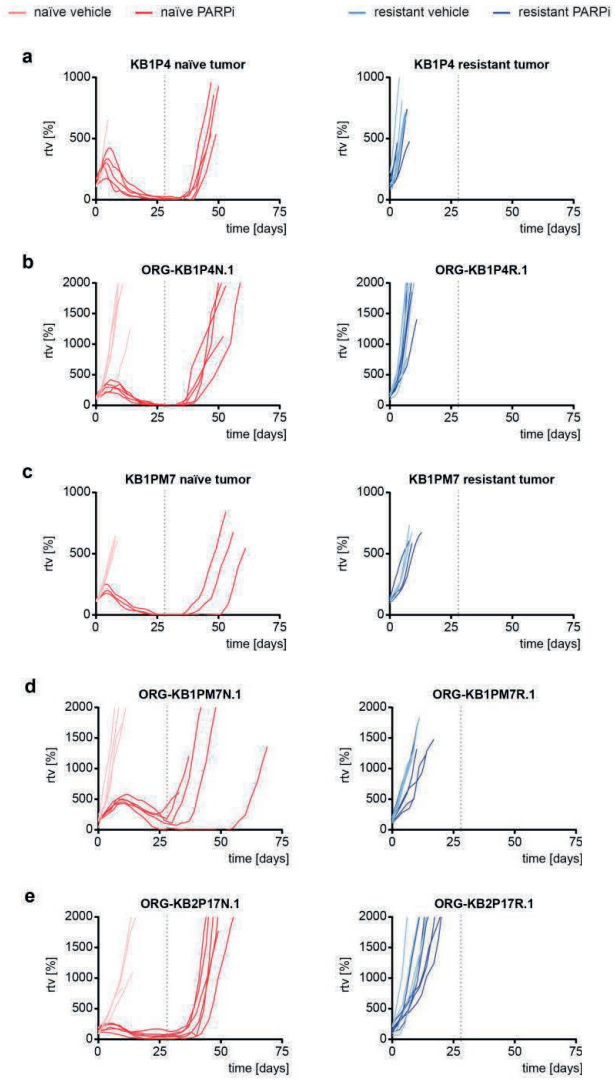
SUPPLEMENTARY FIGURE 3 | Genetic characterization of mouse mammary tumor organoids by DNA copy number profiling. *(A)* Unsupervised hierarchical clustering of a panel of 18 organoid lines and respective original GEMM tumors (extended version of Fig. 1C). *(B)* Unsupervised hierarchical clustering of original GEMM tumor (KB1P), two organoid lines (ORG-KB1P.1, ORG-KB1P.2) and two cell lines derived from the same tumor (independent clones, KB1P-B11 and KB1P-G3, previously described[8]; correlation distance, complete linkage).



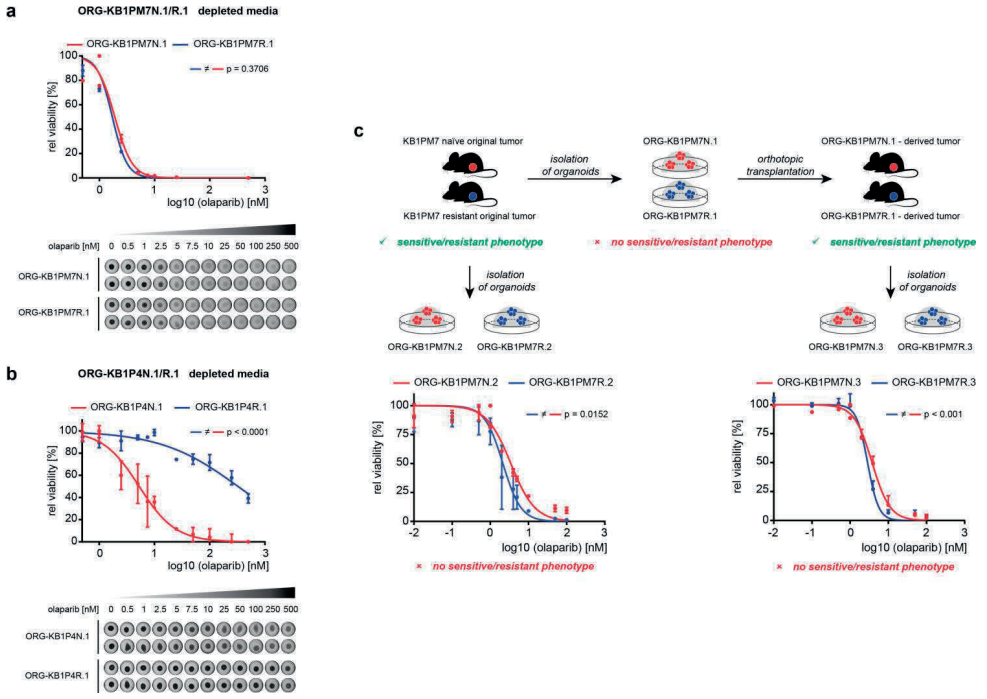
SUPPLEMENTARY FIGURE 4 | Histological characterization of KB1P(M)/KB2P mammary tumor organoids. *(A-C)* Representative images of hematoxylin & eosin (HE) stainings and immunohistochemical analyses of E-cadherin, Vimentin and Keratin-14 expression in KB1P4 *A*, KB1PM7 *B* and KB2P17 *C* GEMM tumors, tumor-derived organoids and organoid-derived tumors. Scale bar, 100 μm.



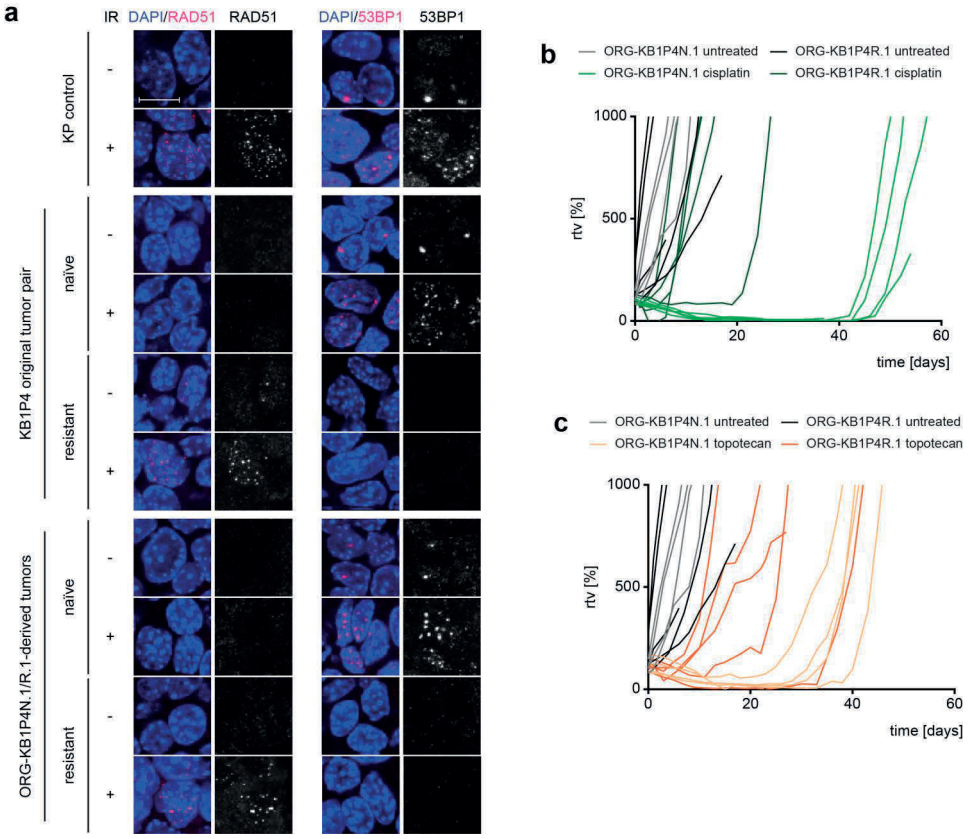
SUPPLEMENTARY FIGURE 5 | Lentiviral transduction of KB1P mammary tumor organoids. Green fluorescent protein (GFP) was introduced into ORG-KB1P4N.1 organoids by lentiviral transduction using pLenti6-GFP at the indicated theoretical multiplicities of infection (MOI). GFP expression was analyzed by flow cytometry 3 days after transduction.



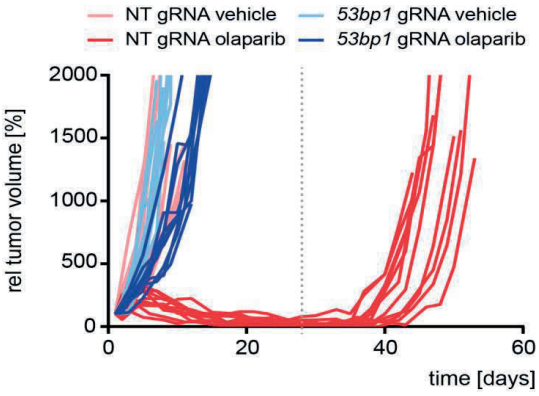
SUPPLEMENTARY FIGURE 6 | Response of KB1P(M) and KB2P tumors to PARPi treatment. (*A-E*) Mice orthotopically transplanted with olaparib-naïve or –resistant KB1P4 tumors (*n* = 2 naïve vehicle, *n* = 5 for other treatment groups) *A*, ORG-KB1P4N.1/R.1 organoids (*n* = 5) *B*, olaparib-naïve or –resistant KB1PM7 tumors (*n* = 4 resistant vehicle, *n* = 3 for other treatment groups) *C*, ORG-KB1PM7N.1/R.1 organoids (*n* = 5) *D* or AZD2461-naïve or –resistant ORG-KB2P17N.1/R.1 organoids (*n* = 4 for vehicle, *n* = 6 for AZD2461) *E* were treated with either vehicle *A-E*, olaparib *A-D* or AZD2461 *E* for 28 consecutive days. End of treatment is indicated by a dotted grid line. Graphs show relative tumor volume (ratio of tumor volume to initial size at start of treatment) as a function of time (see also Fig. 2).



SUPPLEMENTARY FIGURE 7 | Comparison of *in vitro* PARPi response of GEMM tumor-derived organoids. *(A-B) In vitro* response of ORG-KB1PM7N.1/R.1 *A* and ORG-KB1P4N.1/R.1 *B* organoids cultured in media depleted of R-spondin 1, Noggin and EGF as determined by a viability assay. Representative stainings of organoids are shown in duplicate. *P* values were determined by a non-linear regression model and extra sum-square F-test. *(C) In vitro* response of ORG-KB1PM7N.2/R.2 organoids, independently isolated from the original KB1PM7N/R tumors, and ORG-KB1PM7N.3/R.3 organoids, isolated from the vehicle-treated tumors that originated from transplantation of ORG-KB1PM7N.1/R.1 organoids. *P* values were determined as described for *A-B*. Data are presented as mean ± SD for at least 2 independent replicates.



SUPPLEMENTARY FIGURE 8 | ORG-KB1P4R.1-derived tumors preserve PARPi resistance mechanism of the original tumor. *(A)* RAD51 and 53BP1 ionizing radiation-induced foci (IRIF) formation in original KB1P4 olaparib-naïve and -resistant tumors and ORG-KB1P4N.1/R.1-derived tumors 2 hours after irradiation with 15 Gy (IR). A KP tumor was used as a positive control for RAD51 foci formation. Representative microscopic images are shown. Scale bar, 10 μm. See Fig. 3B-C for quantification. *(B-C) In vivo* response of tumors derived from ORG-KB1P4N.1/R.1 to cisplatin (*B*; *n* = 5 naïve vehicle, *n* = 3 resistant vehicle, *n* = 5 naïve/resistant cisplatin) and topotecan (*C*; *n* = 5 naïve vehicle, *n* = 3 resistant vehicle, *n* = 4 naïve topotecan, *n* = 5 resistant topotecan). Data presented as relative tumor volume over time.



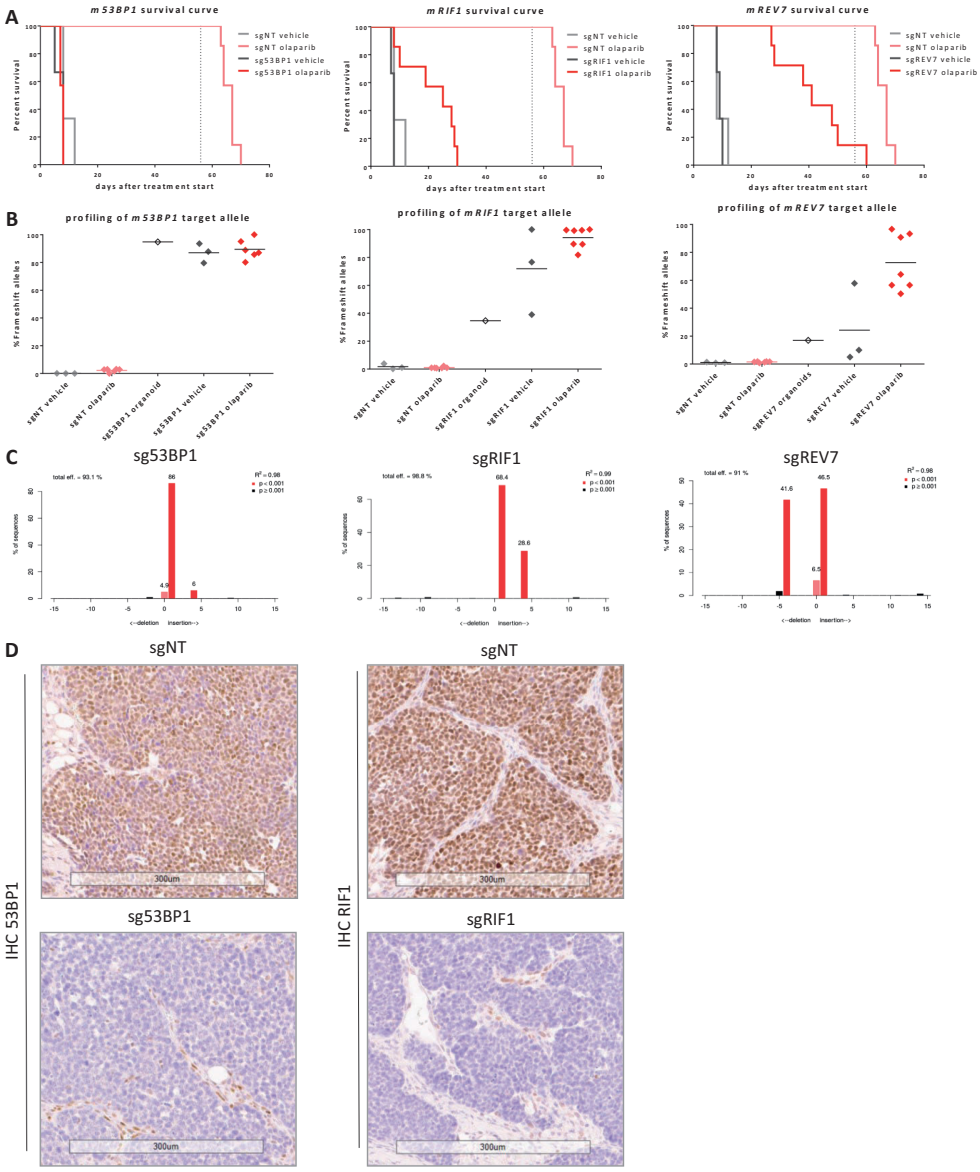
SUPPLEMENTARY FIGURE 9 | Response of genetically modified organoid-derived mammary tumors to olaparib treatment. Mice bearing tumors derived from ORG-KB1PM7N.1 organoids modified *in vitro* by CRISPR/Cas9 using a gRNA targeting *Trp53bp1* (*Trp53bp1* gRNA) or a non-targeting gRNA (NT gRNA). Animals were treated with either vehicle or olaparib for 28 consecutive days (n = 10 per treatment group). End of treatment is indicated by a dotted grid line. Graphs show relative tumor volume (ratio of tumor volume to initial size at start of treatment) as a function of time. See also Fig. 4.

SUPPLEMENTARY TABLE 1 | Overview of tumor outgrowth following transplantation of tumor (ORG-KB1P4N.1) and healthy tissue-derived (N-ORG) organoids at the indicated cell numbers (see also Fig. 1b). Outgrowth rate: values in brackets indicate the number of tumors obtained *vs.* total number of mammary fat pads injected. Time until tumor volume = 75mm^3: mean ± SD. Tumor watch for N-ORG, 70 days.

organoid line	number of cells transplanted	tumor outgrowth rate (flanks/tumors) [%]	time until tumor volume = 75mm³ [days]
ORG- KB-1P4N.1	10^6	100 (4/4)	10 ± 1
	10^5	100 (7/7)	16 ± 4
	10^4	100 (7/7)	25 ± 6
	10^3	90 (9/10)	39 ± 13
	102	20 (2/10)	n.d.
N-ORG	105	0 (0/20)	n.d.
	104	0 (0/14)	n.d.

Addendum

In this study, we present a proof-of-principle experiment to evaluate the effect of a known resistance factor, 53BP1, on PARPi-treatment response *in vivo.* Hereto, CRISPR/Cas9-mediated gene editing was combined with 3D organoid culture technology. We next used this versatile platform to evaluate two other known resistance factors in the 53BP1-pathway, RIF1 and REV7, side-by-side in an isogenic manner. Although the treatment duration has been prolonged to extend the evaluation window, this experiment confirmed that sgNT-targeted organoids remained responsive to continuous olaparib treatment for 56 consecutive days (median survival of 67 days) (Addendum Fig. 1A). In contrast, knock-out of 53BP1 or REV7 induced resistance to treatment with PARPi (median survival of 8 and 41 days, respectively; $P < 0.001$). Through this approach we also provide the first *in vivo* evidence for RIF1 as a driver of resistance to PARi (median survival of 25 days; $P < 0.001$). Profiling of the target allele in resistant tumors confirmed that resistant tumors were hallmarked by non-functional allelic variants (Addendum Fig. 1B-C). This tumor panel also provided sample material to establish an immunohistochemistry (IHC) protocol to stain endogenous mouse RIF1 protein on formalin-fixed and EAF-fixed material, allowing us to verify 53BP1 and RIF1 protein depletion in resistant tumors. Indeed, resistant sg53BP1- or sgRIF1-targeted tumors showed clear loss-of-53BP1- or RIF1 protein by IHC, respectively (Addendum Fig. 1D). An IHC protocol to stain for endogenous mouse REV7 protein could not be established. Subsequently, RIF1 IHC has been performed on a panel of KB1P(M) tumors with spontaneously acquired resistance to PARPi-treatment and observed that a subset of these tumors displayed loss-of-RIF1 expression (data not shown), suggesting that a subset of these tumors may have developed spontaneous PARPi resistance through inactivation of RIF1.



ADDENDUM FIGURE 1 | isogenic *in vivo* evaluation of 53BP1-pathway factors on PARPi-response. *(A)* Kaplan-Meier curves indicating the survival of mice bearing tumors targeted by the indicated sgRNA. Animals were treated with vehicle (n = 3) or olaparib (n = 7) for 56 consecutive days (indicated by the dashed line) and animals were sacrificed when tumors reached a size of ≥ 1500 mm^3. P-value was calculated using the log rank test (Mantel-Cox). *(B)* Frequency of frameshift indels in indicated tumors. *(C)* example of the allele distribution of a resistant tumor targeted by the indicated sgRNA. *(D)* Immunohistochemistry analysis of 53BP1 or RIF1 expression in resistant tumors targeted with the indicated sgRNA. Scale bar represents 300 µm.